Monthly Notices of the ROYAL ASTRONOMICAL SOCIETY

MNRAS **536,** 408–421 (2025) https://doi.org/10.1093/mnras/stae2585
Advance Access publication 2024 November 15

SN 1054 as a pulsar-driven supernova: implications for the crab pulsar and remnant evolution

Conor M. B. Omand [1,2]★ Nikhil Sarin [3,4] and Tea Temim [5]

[1]*Astrophysics Research Institute, Liverpool John Moores University, Liverpool Science Park IC2, 146 Brownlow Hill, Liverpool L3 5RF, UK*
[2]*The Oskar Klein Centre, Department of Astronomy, Stockholm University, AlbaNova, SE-106 91 Stockholm, Sweden*
[3]*The Oskar Klein Centre, Department of Physics, Stockholm University, AlbaNova, SE-106 91 Stockholm, Sweden*
[4]*Nordita, Stockholm University and KTH Royal Institute of Technology, Hannes Alfvéns väg 12, SE-106 91 Stockholm, Sweden*
[5]*Department of Astrophysical Sciences, Princeton University, 4 Ivy Lane, Princeton, NJ 08544, USA*

Accepted 2024 November 13. Received 2024 November 13; in original form 2024 April 29

ABSTRACT

One of the most studied objects in astronomy, the Crab Nebula, is the remnant of the historical supernova SN 1054. Historical observations of the supernova imply a typical supernova luminosity, but contemporary observations of the remnant imply a low explosion energy and low ejecta kinetic energy. These observations are incompatible with a standard ^{56}Ni-powered supernova, hinting at an an alternate power source such as circumstellar interaction or a central engine. We examine SN 1054 using a pulsar-driven supernova model, similar to those used for superluminous supernovae. The model can reproduce the luminosity and velocity of SN 1054 for an initial spin period of ∼14 ms and an initial dipole magnetic field of 10^{14-15} G. We discuss the implications of these results, including the evolution of the Crab pulsar, the evolution of the remnant structure, formation of filaments, and limits on freely expanding ejecta. We discuss how our model could be tested further through potential light echo photometry and spectroscopy, as well as the modern analogues of SN 1054.

Key words: stars: magnetars – pulsars: individual: Crab pulsar – supernovae: individual: SN 1054 – ISM: supernova remnants.

1 INTRODUCTION

The Crab Nebula is one of the most well-studied astronomical objects in the sky (e.g. Davidson & Fesen 1985; Hester 2008; Bühler & Blandford 2014, and references therein). It is one of a few remnants where the supernova (SN 1054) is recorded in historical records, and thus the age of the remnant is well constrained (Clark & Stephenson 1977). However, despite extensive studies, many questions still remain, such as the progenitor of the explosion and the explosion mechanism. These questions are mostly driven by the unusually low kinetic energy inferred from studies of the remnant (MacAlpine et al. 1989; Bietenholz et al. 1991; Fesen, Shull & Hurford 1997; Smith 2003) despite the supernova being consistent with the luminosity of typical supernovae.

SN 1054 was observed for around two years by astronomers in Japan, China, and parts of Europe (Clark & Stephenson 1977; Collins, Claspy & Martin 1999). From records in China and Japan, the supernova was visible during the day for 23 d and during the night for around 650 d (Clark & Stephenson 1977), although some European records suggest the supernova may have been bright enough to see during the day for several months (Collins et al. 1999). The presence of a pulsar and detection of several solar masses of material in filaments makes it clear that SN 1054 was a core-collapse supernova, and the detection of a substantial amount of hydrogen in the filaments (Davidson & Fesen 1985) implies a Type II classification (Dessart et al. 2012; Hachinger et al. 2012).

The low distance to the Crab has allowed detailed observations of the structure of the Crab system, which consists of the pulsar, synchrotron nebula, thermal filaments, and freely expanding ejecta (Hester 2008). The observed velocities of the filaments range between ∼ 700–1800 km s^{-1}, with a characteristic value of ∼ 1500 km s^{-1} (Clark et al. 1983; Bietenholz et al. 1991; Temim et al. 2006). These filaments show complex structures that likely arise from Rayleigh–Taylor instabilities at the interface between the synchrotron nebula and ejecta (Davidson & Fesen 1985; Hester 2008). The inferred kinetic energy of these filaments is $\lesssim 10^{50}$ erg. The freely expanding ejecta beyond the edge of the easily visible nebula was detected between ∼1200 and 2500 km s^{-1} in C IVλ1550 absorption (Sollerman et al. 2000), although no forward shock has been detected in either radio or X-ray beyond the edge of the synchrotron nebula and filaments (Mauche & Gorenstein 1989; Frail et al. 1995; Predehl & Schmitt 1995; Seward, Gorenstein & Smith 2006). The material detected by C IV absorption is consistent with a kinetic energy of 10^{51} erg, but only for shallow density profiles (Sollerman et al. 2000; Hester 2008).

What could have powered the unusually bright supernova luminosity? The low inferred kinetic energy of the filaments has led to suggestions of SN 1054 being an electron-capture supernova (ECSN; Miyaji et al. 1980), which involves the collapse of an oxygen-neon-magnesium core in an 8–10 $M_\odot$ progenitor (Nomoto et al. 1982; Nomoto 1987). This produces an explosion with a typical energy of 10^{50} erg, compared to the canonical 10^{51} erg from the collapse

★ E-mail: c.m.omand@ljmu.ac.uk

of an iron core. However, low-energy explosion models, including ECSNe, are typically sub-luminous due to the low quantity of ^{56}Ni synthesized during the explosion (Kitaura, Janka & Hillebrandt 2006). SN 2018zd has also been suggested to be an ECSN (Zhang et al. 2020; Hiramatsu et al. 2021), although further studies of both the Crab Nebula and SN 2018zd have favoured a low-mass core-collapse interpretation (Callis et al. 2021; Temim et al. 2024). Some studies propose that the luminosity could be powered by shock interaction with circumstellar medium (CSM; Fesen et al. 1997; Sollerman, Kozma & Lundqvist 2001; Smith 2013), although this is disfavoured by some models (Hester 2008; Yang & Chevalier 2015) due to the required mass limiting the presence of freely expanding ejecta. Other studies propose that the central pulsar could have supplied the required energy (Sollerman et al. 2001; Li, Yu & Huang 2015).

The discussion of CSM and pulsar-power draws parallels to another class of transients; superluminous supernovae (SLSNe). Photometric observations are unable to distinguish between the power sources (e.g. Chen et al. 2023b), and therefore, other information, such as nebular spectra (Chevalier & Fransson 1992; Jerkstrand et al. 2017; Dessart 2019; Omand & Jerkstrand 2023), polarization (Inserra et al. 2016; Saito et al. 2020; Poidevin et al. 2022, 2023; Pursiainen et al. 2022, 2023), infrared emission (Omand, Kashiyama & Murase 2019; Chen et al. 2021; Sun, Xiao & Li 2022), and radio emission (Murase et al. 2015; Omand, Kashiyama & Murase 2018; Eftekhari et al. 2019; Law et al. 2019; Mondal et al. 2020; Eftekhari et al. 2021; Margutti et al. 2023) are used to try and diagnose the power sources of these supernovae. While we have access to extensive multiwavelength observations about the Crab, models of pulsar-driven supernovae generally do not make predictions out to 1000 yr due to the extragalactic distances of those sources.

The properties of the Crab pulsar and pulsar wind nebula (PWN) have been extensively studied. The spin frequency and frequency derivative are 30 Hz and -4×10^{-10} Hz s^{-1}, respectively (Staelin & Reifenstein 1968; Lyne, Pritchard & Graham Smith 1993; Lyne et al. 2015). The characteristic magnetic field of the pulsar is $\sim 8 \times 10^{12}$ G, assuming $B_c = 6.4 \times 10^{19}\sqrt{P\dot{P}}$ G for pure magnetic dipole losses (Kou & Tong 2015), and the current braking index n is 2.51 $\pm$ 0.01 (Lyne et al. 1993). Estimates of the initial pulsar spin period are usually in the range of 15–20 ms (e.g. Kou & Tong 2015), but a study of the electron spectrum estimated a much faster initial spin of around 3–5 ms (Atoyan 1999). A pulsar spinning at this rate could potentially supply the required energy to produce the luminosity observed in SN 1054.

In this work, we examine SN 1054 under the lens of the pulsar-driven supernova model to determine whether this scenario is consistent with the observed supernova and remnant properties and estimate the initial properties of the Crab pulsar and PWN. We also examine the implications of a pulsar engine on the evolution of the pulsar and the supernova remnant. In Section 2, we overview the model and constraints from observations. In Sections 3 and 4, we present the results from our analysis and discuss their implications. Lastly, in Section 5, we summarize our findings.

2 MODEL AND CONSTRAINTS

2.1 Model overview

The model we use is the generalized magnetar-driven supernova model first presented in Omand & Sarin (2024), based on models of magnetar-driven kilonovae (Yu, Zhang & Gao 2013; Metzger 2019; Sarin et al. 2022). We present a brief summary of the key components of the model here.

The spin-down luminosity of the pulsar is

$$L_{\rm SD}(t) = L_0 \left(1 + \frac{t}{t_{\rm SD}}\right)^{\frac{1+n}{1-n}}, \tag{1}$$

where L_0 is the initial spin-down luminosity, $t_{\rm SD}$ is the spin-down time-scale, and n is the braking index defined from $\dot{\Omega} \propto -\Omega^n$. The total rotational energy is

$$E_{\rm rot} = \frac{n-1}{2} L_0 t_{\rm SD}. \tag{2}$$

The evolution of the internal energy of the ejecta is

$$\frac{dE_{\rm int}}{dt} = \xi(L_{\rm SD} + L_{\rm ra}) - L_{\rm bol} - \mathcal{P}\frac{d\mathcal{V}}{dt}, \tag{3}$$

where $L_{\rm ra}$ and $L_{\rm bol}$ are the radioactive power and emitted bolometric luminosity, respectively, $\mathcal{P}$ and $\mathcal{V}$ are the pressure and volume of the ejecta, and

$$\xi = 1 - e^{-At^{-2}}, \tag{4}$$

is the fraction of spin-down luminosity injected into the ejecta (Wang et al. 2015), where

$$A = \frac{3\kappa_\gamma M_{\rm ej}}{4\pi v_{\rm ej}^2} \tag{5}$$

is the leakage parameter and κ_γ is the gamma-ray opacity of the ejecta. We assume all energy from radioactive decay is emitted as gamma rays and that the ejecta has the same gamma-ray opacity for both radioactive heating and magnetar heating.

The ejected material accelerates with

$$\frac{dv_{\rm ej}}{dt} = \frac{E_{\rm int}}{M_{\rm ej} R_{\rm ej}} \tag{6}$$

due to the interaction with the pulsar wind nebula, and the supernova bolometric luminosity is

$$L_{\rm bol} = \frac{E_{\rm int} c}{\tau R_{\rm ej}} = \frac{E_{\rm int} t}{t_{\rm dif}^2} \qquad (t \le t_\tau), \tag{7}$$

$$= \frac{E_{\rm int} c}{R_{\rm ej}}, \qquad (t > t_\tau), \tag{8}$$

where

$$\tau = \frac{\kappa M_{\rm ej} R_{\rm ej}}{\mathcal{V}} \tag{9}$$

is the optical depth of the ejecta, κ is the optical ejecta opacity,

$$t_{\rm dif} = \left(\frac{\tau R_{\rm ej} t}{c}\right)^{1/2} \tag{10}$$

is the effective diffusion time, and t_τ is the time when $\tau = 1$.

The photospheric temperature is

$$T_{\rm phot}(t) = \begin{cases} \left(\frac{L_{\rm bol}(t)}{4\pi\sigma R_{\rm ej}^2}\right)^{1/4} & \text{for } \left(\frac{L_{\rm bol}(t)}{4\pi\sigma R_{\rm ej}^2}\right)^{1/4} > T_{\rm min}, \\ T_{\rm min} & \text{for } \left(\frac{L_{\rm bol}(t)}{4\pi\sigma R_{\rm ej}^2}\right)^{1/4} \le T_{\rm min} \end{cases} \tag{11}$$

where $T_{\rm min}$ is the temperature of the supernova after the photosphere begins to recede.

The constant opacity κ is justified while the ejecta is ionized, but this opacity will drop once the photospheric temperature hits the ionization temperature ($\sim$6000 K) and the ejecta starts to recombine (Popov 1993; Dexter & Kasen 2013; Tsuna et al. 2024).

Table 1. The parameters and priors used in this study. Priors are either uniform (U) or log-uniform (L). The values shown for the posterior are the mean and 1σ uncertainties. Posterior values denoted with L are given in log-space. The full posterior is shown in Appendix A.

Parameter	Definition	Units	Prior/value	Posterior values
D	Distance	kpc	U [1.72, 2.12]	$1.92^{+0.12}_{-0.13}$
L_0	Initial magnetar spin-down luminosity	erg s^{-1}	L [10^{39}, 10^{46}]	$L(44.50^{+0.97}_{-1.45})$
$t_{\rm SD}$	Spin-down time	s	L [10^{4}, 10^{10}]	$L(5.73^{+1.12}_{-0.86})$
n	Magnetar braking index		3	
$f_{\rm Ni}$	Ejecta nickel mass fraction		0.005	
$M_{\rm ej}$	Ejecta mass	M$_\odot$	U [3, 9]	$5.24^{+2.09}_{-1.55}$
$E_{\rm SN}$	Supernova explosion energy	10^{49} erg	U [1, 10]	$5.53^{+2.82}_{-2.80}$
κ	Ejecta optical opacity	cm^2 g^{-1}	0.34	
κ_γ	Ejecta gamma-ray opacity	cm^2 g^{-1}	L [10^{-4}, 10^{4}]	$L(-2.63^{+3.52}_{-0.98})$
$T_{\rm min}$	Photospheric plateau temperature	1000 K	U [0.5, 10]	$2.82^{+4.60}_{-1.23}$
	Explosion time	days	U [−300,−0.1]	$-183.29^{+105.12}_{-72.85}$

Recombination effects stop being important once the diffusion time $t_{\rm dif}$ becomes much smaller than the dynamical time. We do not include recombination effects in this model, which we note as a potential caveat of our fits.

2.2 Priors and constraints

The historical observations of SN 1054 (Clark & Stephenson 1977; Collins et al. 1999) can provide two constraints on the luminosity of the supernova at various times. The first is that the supernova was visible during the day for at least 23 d and the second is that the supernova was visible during the night for around 650 d (Clark & Stephenson 1977). After accounting for extinction (Miller 1973), this gives apparent V-band magnitudes of roughly −4.5 and 6.0, respectively, with uncertainties of ± 0.5–0.8 mag (Collins et al. 1999).

The priors used in inference are determined by constraints from observations of the Crab Nebula and from previous modeling of different supernovae. The most constraining distance estimate to the Crab Nebula, as determined from very-long-baseline interferometry (VLBI) measurements of a giant pulse, is $1.90^{+0.22}_{-0.18}$ kpc (Lin et al. 2023). The ejecta mass estimated from an optical study of neutral and ionized gas in the Crab Nebula is 4.6 ± 1.8 M$_\odot$ (Fesen et al. 1997), although the authors suggest that up to 4 M$_\odot$ could remain undetected. Observations of absorption in the freely expanding ejecta outside the nebula suggest that component has $\gtrsim$1.7 M$_\odot$ (Sollerman et al. 2000), and later radiative transfer simulations of the gas and dust content of the Crab find 7.2 ± 0.5 M$_\odot$ of material should be present within all the ejected material (Owen & Barlow 2015). Given these estimates, we conservatively set the limits of the prior to be between 3 and 9 M$_\odot$. The explosion energy, estimated from the 1500 km s^{-1} velocity of the pulsar bubble (Bietenholz et al. 1991), must be much lower than the canonical 10^{51} erg value for typical core-collapse supernovae; a value of 10^{50} erg is typical from simulations of the collapse of low-mass stars (Nomoto et al. 1982; Nomoto 1987), so we set the prior between 10^{49} erg and 10^{50} erg. This assumes that the component of the ejecta outside the filaments does not carry significantly more kinetic energy that the filaments themselves. The amount of ^{56}Ni synthesized in these low energy explosions is generally not more than a few 0.01 M$_\odot$ (Kitaura et al. 2006), so we fix the nickel fraction (i.e. the fraction of the total ejecta that is nickel) to 0.005. However, we note that such small quantity of nickel does not significantly contribute to the light curve.

The expected spin-down time of the Crab pulsar is ∼30 yr if the initial pulsar spin is ∼5 ms (Atoyan 1999) and the magnetic field stays constant over time, and larger if the pulsar is spinning slower. Since this time-scale is much larger than the time-scale that the supernova was observed for (<2 yr), the spin-down luminosity (equation 1) should not evolve significantly over that time ($L_{\rm SD}(t) \approx L_0$ for $t \ll t_{\rm SD}$). This means that we can not infer either the spin-down time-scale or braking index (which may be significantly different from the currently measured value) unless the spin-down time-scale is significantly smaller than previously thought. A significantly smaller spin-down time-scale would imply a higher magnetic field than currently inferred. We set a prior between 10^4 and 10^{10} s for the spin-down time to determine if the spin-down time can be short, but keep n fixed to 3 (the exact value of n does not strongly affect our results, see Appendix A for details). The prior on L_0 ranges from 10^{39} to 10^{46} erg s^{-1}, spanning the range from where the pulsar has almost no effect on the supernova to where the pulsar luminosity is consistent with a superluminous supernova (Omand & Sarin 2024). The current spin period of the Crab pulsar is 33 ms (Lyne et al. 1993), which gives the pulsar a current rotational energy of $\sim 2 \times 10^{49}$ erg for a 1.4 $M_\odot$, 12 km radius neutron star; which we use to motivate the lower limit on the prior for L_0 and $t_{\rm SD}$.

The final quantities to infer are the optical and gamma-ray opacities, κ and κ_γ, respectively, the plateau temperature $T_{\rm min}$, and the explosion time. The optical opacity prior is set to 0.34 cm^2 g^{-1}, the typical value for a hydrogen-rich supernova (Inserra et al. 2018). The prior on gamma-ray opacity is not well constrained, and so a wide prior of 10^{-4}–10^4 cm^2 g^{-1} is used, although recent work suggests values of $\sim 10^{-2}$–1 cm^2 g^{-1} are suitable for synchrotron nebulae (Vurm & Metzger 2021). The plateau temperature, which is the temperature of the ejecta when the photosphere starts to recede, could be significantly lower than the typical value of 6000 K from SLSNe (Nicholl, Guillochon & Berger 2017), and we take a prior from 500–10 000 K to reflect this. It is worth noting that fixing the plateau temperature to 6000 K does not strongly affect our results (see Appendix A). The unknown explosion time is sampled uniform prior of up to 300 d before the point where the supernova faded from the daytime sky. All of the parameters and priors are summarized in Table 1.

3 RESULTS

We fit the historical observations of SN 1054 using the model and priors described in Section 2. Inference is performed using the

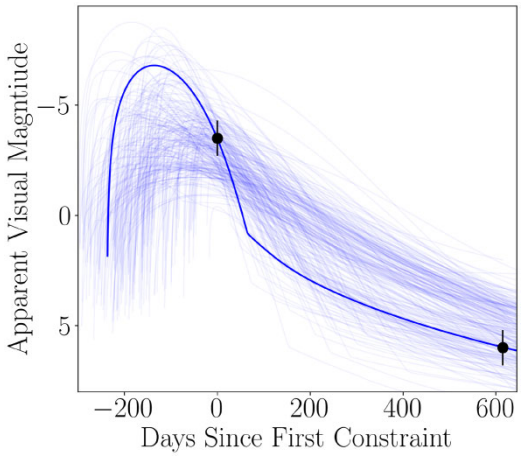

Figure 1. Fitted dust-corrected light curves for SN 1054. The thin lines indicate 300 models drawn randomly from the posterior, and the thick line indicates the most likely model. Since we sample over distance, the distance modulus ($m_V - M_V$) varies between 11.2 and 11.6.

open-source software package REDBACK (Sarin et al. 2024) with the PYMULTINEST sampler (Buchner et al. 2014) implemented in BILBY (Ashton et al. 2019). We sample in magnitude with a Gaussian likelihood. We constrain the priors for L_0 and $t_{\rm SD}$ such that the initial rotational energy of the pulsar is higher than 10^{49} erg, which is a conservative estimate of the current pulsar rotational energy.

The light curve fit is shown in Fig. 1 and the posterior in Appendix A. The only parameters that matter for determining the initial total energy of the pulsar wind nebula are L_0, the initial spin-down luminosity, and $t_{\rm SD}$, the pulsar spin-down time. The initial spin-down luminosity is most likely $\sim 10^{43-45.5}$ erg s^{-1}, which is similar to the initial spin-down luminosity of pulsars that power SLSNe such as SN 2015bn (Omand & Sarin 2024). This value is a factor $\gtrsim$10 more than the estimated initial radioactive luminosity, and radioactivity also decays off more quickly than the magnetar luminosity. Therefore, the magnetar will always be the dominant contributor to the supernova internal energy (equation 3). The spin-down time-scale is most likely around $1 - 100$ d, much lower than the expected 30 yr for a fast-rotating pulsar with constant magnetic field (Atoyan 1999). This likely implies that the magnetic field must have initially been much stronger than the current inferred field strength; we discuss this further in Section 4.1.

The fitted light curves show a broad distribution in both peak luminosity and explosion time due to the low number of constraining data. It is unclear from historical constraints whether the supernova could have had a peak magnitude much brighter than −5 or an explosion time in the winter of 1054, since the first known records of a possible supernova sighting are in April (Collins et al. 1999). The posterior for the explosion time does not show a strong correlation with any other parameters (Fig. A1), while the distribution of peak luminosities shows slight correlations with L_0 and $t_{\rm SD}$. If an upper limit were imposed on the peak luminosity, this would push the posterior towards higher L_0 and lower $t_{\rm SD}$, in agreement with the general behaviour found in Omand & Sarin (2024), and imply an even higher initial poloidal magnetic field. None of our results or their implications would be significantly affected by peak luminosity or explosion time constraints.

The ratio of the calculated diffusion time from the model at the time of the first observation to the dynamical time of the first

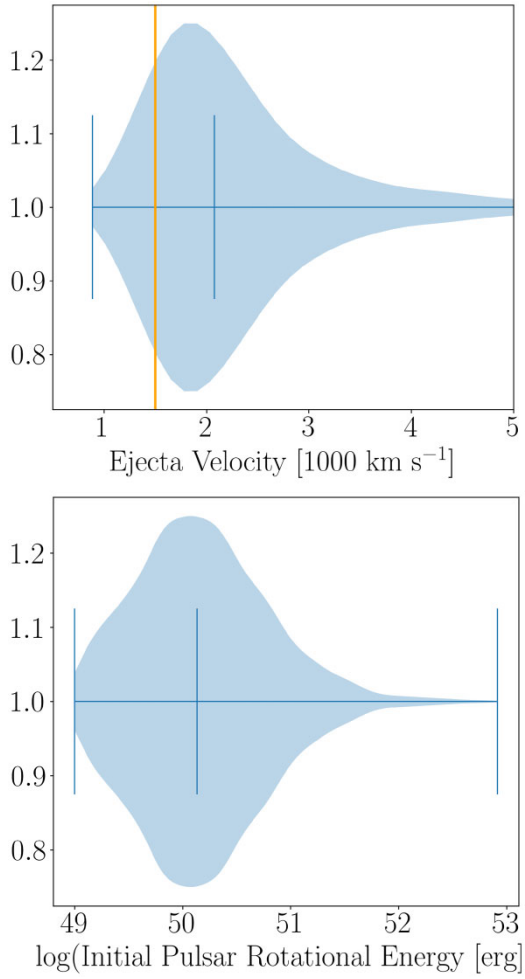

Figure 2. (Top) The distribution of final ejecta velocities inferred for SN 1054, with the value of the Crab Nebula forward shock (Bietenholz et al. 1991) shown with a line. (Bottom) The distribution of initial pulsar spin-down energies inferred for SN 1054. The outer bounds and median values for each distribution are shown with blue lines.

observation is <1/2 for 68 per cent of the posterior and <1/10 for 36 per cent of the posterior. About 18 per cent of the posterior has $T_{\rm phot} > 6000$ K at the time of the first observation. Assuming $t_{\rm dyn}/t_{\rm dif} > 2$ is a reasonable criterion for when recombination effects become unimportant, we find that only ∼32 per cent of the posterior would be affected by recombination at the first observation epoch. Assuming recombination is important only when both $t_{\rm dyn}/t_{\rm dif} < 2$ and $T_{\rm phot} < 6000$ K, we still find that ∼32 per cent of the posterior would be affected by recombination at the first observation epoch, since all of the samples with high diffusion time also have low photospheric temperatures. None of the supernovae from our posterior are affected by recombination at the second epoch.

The posterior distributions of the final ejecta velocity and initial pulsar rotational energy, assuming vacuum dipole spin-down, are shown in Fig. 2. The ejecta velocity is defined here as the velocity where $E_{\rm kin} = \frac{1}{2} M_{\rm ej} v_{\rm ej}^2$; this is sometimes known as the scaling velocity or bulk ejecta velocity. The median values of the two distributions are 2000 km s^{-1} and 1.4×10^{50} erg, respectively. Most

of the inferred ejecta velocities are only slightly higher than the measured value of 1500 km s^{-1} of the forward shock (Bietenholz et al. 1991), although only 14 per cent of the distribution is below that value. The initial rotational energy peaks at only slightly higher than the maximum value from the explosion energy prior of 10^{50} erg, and is similar to the values inferred for the SN Ic-BL SN 2007ru and USSN iPTF14gqr and lower than those inferred for the SLSN SN 2015bn and FBOT ZTF20acigmel (Omand & Sarin 2024). Using scaling relations for a 1.4 $M_\odot$, 12 km neutron star

$$E_{\rm rot} = 2.6 \times 10^{52} P_{0,-3}^{-2} \text{ erg}, \tag{12}$$

$$L_0 = 2.0 \times 10^{47} P_{0,-3}^{-4} B_{14}^{2} \text{ erg s}^{-1}, \tag{13}$$

$$t_{\rm SD} = 1.3 \times 10^{5} P_{0,-3}^{2} B_{14}^{-2} \text{ s}, \tag{14}$$

to convert this energy into an initial spin period gives $P_0 = 16.3 \pm 10.5$ ms with a median value of 13.8 ms, which is consistent with both the values of 15–20 ms derived from extrapolating backwards from current conditions (See Appendix B) and the value of 5 ms estimated from the radio spectrum of the pulsar wind nebula (Atoyan 1999).

The 2D posterior distributions of ejecta velocity $v_{\rm ej}$, supernova explosion energy $E_{\rm SN}$, and initial pulsar rotational energy $E_{\rm rot}$ are shown in Fig. 3. Both $E_{\rm SN}$ and $E_{\rm rot}$ show weak correlations with $v_{\rm ej}$, while the two energies are not strongly correlated with each other. Most models with explosion energies close to 10^{50} erg show velocities higher than 1500 km s^{-1}, justifying the upper limit of the explosion energy prior. If the posteriors were constrained to have velocities lower than this limit, the explosion energy would likely have $E_{\rm SN} \lesssim 4 \times 10^{49}$ erg, while the rotational energy would roughly lie between 5 and 10 $\times 10^{49}$ erg, giving a spin period of 16–22 ms. It is worth noting that the supernova explosion energy is not well constrained on its own, and only correlates with the ejecta velocity. Thus, our model can not shed light into the explosion mechanism or distinguish between electron capture and iron-core collapse explosions. Examining the correlation in the energies shows that most of the posterior, 75 per cent, has $E_{\rm rot} > E_{\rm SN}$, and this percentage will rise when selecting for lower velocity models. Supernovae with $E_{\rm rot} > E_{\rm SN}$ undergo blowout, where the PWN forward shock can expand past the inner region of the ejecta, changing the structure of the ejecta and remnant; we discuss this further in Section 4.2.

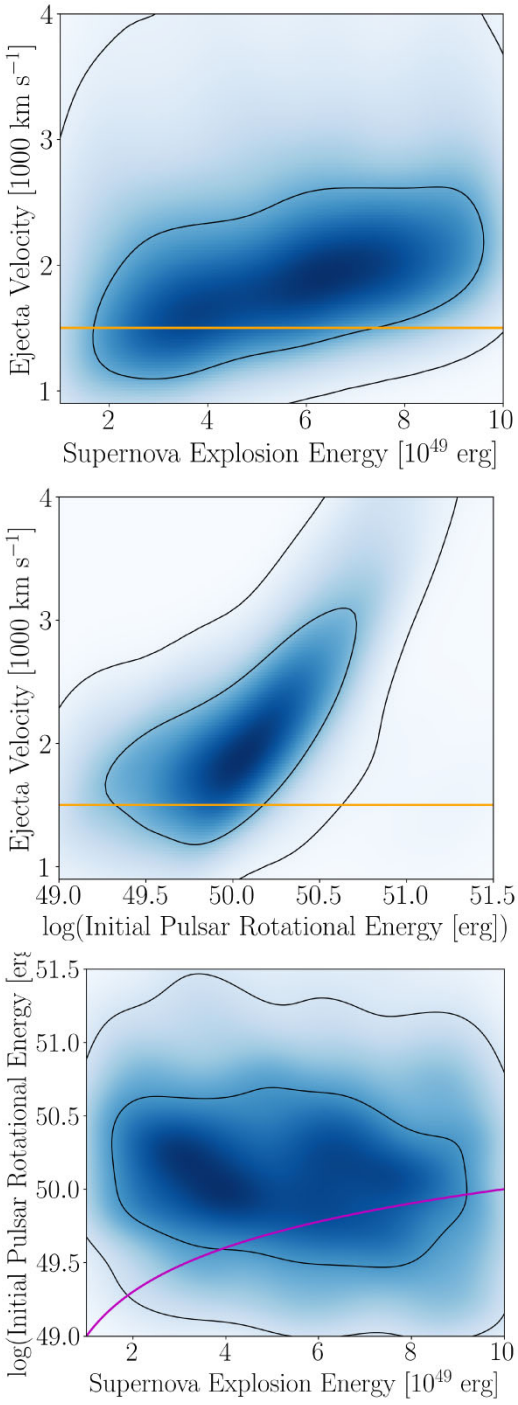

Figure 3. The 2D posterior distributions of ejecta velocity $v_{\rm ej}$, supernova explosion energy $E_{\rm SN}$, and initial pulsar rotational energy $E_{\rm rot}$. The black contours encompass the 50 and 90 per cent credible intervals. The thick lines in the top and middle figures show the velocity of the Crab Nebula forward shock (Bietenholz et al. 1991), and the thick line in the bottom figure shows where $E_{\rm rot} = E_{\rm SN}$. Everything above the line in the bottom figure is expected to exhibit blowout (Blondin & Chevalier 2017).

4 IMPLICATIONS

4.1 Evolution of the Pulsar

The simple theory for the evolution of neutron stars is that they are born with rapid spins, and spin-down through vacuum dipole radiation with a constant magnetic field (Pacini 1967; Borghese 2023). On a period–period derivative ($P\dot{P}$) diagram, this translates into neutron stars being on on the top left of the $P\dot{P}$ diagram and decaying down towards the bottom right on lines of constant magnetic fields.

In Fig. 4, we show a $P\dot{P}$ diagram with the current location of the Crab pulsar (in blue), the inferred location of the pulsar at birth (solid red for the mean of the posterior, with the contour encompassing the 95 per cent credible interval), and the locations of other pulsars obtained from the ATNF catalog (Manchester et al. 2005) via the package PSRQPY (Pitkin 2018) in grey. We also show lines of characteristic ages, constant magnetic fields, and the region below the pulsar 'death line' indicated in yellow. Given the inferred location at birth of the Crab pulsar, the canonical model for neutron star evolution would predict that it evolves along a diagonal line;

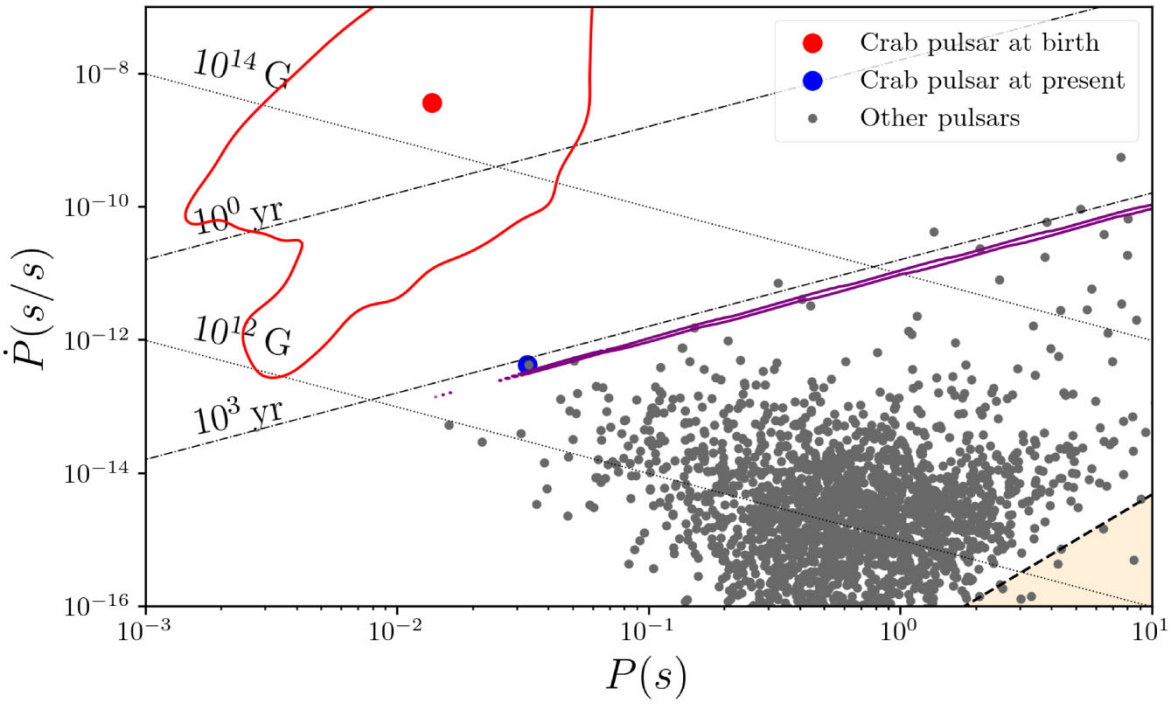

Figure 4. Period and Period derivative $P\dot{P}$ diagram showing the inferred birth and present locations of the Crab pulsar, and other pulsars in the ATNF catalogue gathered via the PSRQPY package (Pitkin 2018). The solid line in the upper left indicates the 95 per cent credible interval of the posterior density distribution. The dots in the middle indicate the 95 per cent credible interval of the predicted present day locations of the posterior after undergoing vacuum dipole spin-down and Ohmic dissipation. We also show lines of characteristic ages, constant magnetic fields, and the region below the pulsar 'death line' indicated at the bottom right of the figure.

spinning down but remaining above the 10^{14} G magnetic-field line and would be more consistent with the location at present day of other 'magnetars' rather than its true current location around other pulsars. This would seem alarming but the simple theory described above is known to be incorrect in a multitude of ways. For example, neutron star magnetic fields are expected to decay due to ohmic dissipation (Igoshev, Popov & Hollerbach 2021), and neutron stars, especially newly born neutron stars, are expected to spin-down through mechanisms other than just vacuum dipole radiation (Melatos 1999; Lasky et al. 2017; Sarin et al. 2018; Sarin, Lasky & Ashton 2020). Another theory, motivated by detailed magnetohydrodynamic simulations suggests that neutron stars are not in fact born with high poloidal (external) magnetic fields but rather small-scale turbulent magnetic fields that later grow to large-scales via an inverse cascade (Sarin, Brandenburg & Haskell 2023). We note that the latter would be at odds with the model we used to fit the historic supernova observations. Given we have, in theory, the location of the Crab pulsar at two evolutionary stages, it is tempting to attempt to interpret how the Crab pulsar must have evolved. We of course, do emphasize that the inferred posterior on the birth location is broad, as expected, such that a simple vacuum dipole radiation model with no evolution of the large-scale magnetic field, need not be ruled out.

The disparity in terms of magnetic fields suggested by the birth and present day location, immediately suggests that the magnetic field must have decayed over the ≈ 1000 yrs since the supernova. The decay of the large-scale, poloidal magnetic field under ohmic dissipation is expected to follow (Pons & Geppert 2007; Sarin et al. 2023)

$$B_{\rm p} = \frac{B_{\rm p,0}}{(1 + t/\tau)^{\alpha}}, \tag{15}$$

where the exponent, $\alpha \sim 1.3$, and $\tau = 800$ yr is the time-scale when the magnetic-field starts to decay. Assuming this magnetic-field evolution, and for simplicity, vacuum-dipole radiation, we evolve the inferred birth location posteriors forward in time till present day. These projected present-day locations are shown in purple (as a 95 per cent credible interval region). The projected locations of the crab pulsar on the $P\dot{P}$ diagram suggest two modes, one that would place the crab pulsar more in line with Galactic magnetars, and another that would be more consistent with the true, present-day location of the crab pulsar. The former mode can be dismissed entirely (at least under the assumption of vacuum dipole spin-down and Ohmic dissipation with the above parameters). However, the consistency of the latter mode is tantalising, suggesting some dissipation of the poloidal magnetic field of the crab pulsar beginning in the last ≈ 200 yr. We note that the values chosen for the decay time-scale and exponent above are inconsistent with expectations of Ohmic dissipation from simulations (Pons & Geppert 2007). However, the general decay behaviour could be recreated through other scenarios such as fall-back accretion. Moreover, inclusion of other more complex spin-down mechanisms, such as gravitational waves could further reconcile the differences from the magnetic-field decay behaviour compared to numerical simulations.

Several mechanisms for magnetic field amplification have been suggested to explain the origin of magnetar-strength magnetic fields.

Field amplification from convective dynamos (Raynaud et al. 2020), magnetorotational instability-driven turbulent dynamos (Reboul-Salze et al. 2021; Guilet et al. 2022), and $\alpha\Omega$ dynamos (Reboul-Salze et al. 2022) can amplify the dipole component of the magnetic field up to $\sim 10^{15}$ G after the proto-neutron star contracts for an initial period $\sim$1 ms. However, these amplification mechanisms scale down as the neutron star spin period increases, meaning they likely could not reproduce the birth properties of the Crab pulsar over a majority of the $P\dot{P}$ posterior. Supernova fallback can also trigger a Tayler–Spruit dynamo in slower rotating proto-neutron stars (Barrère et al. 2022, 2023). Depending on how the field saturates, dipole fields of $\sim 10^{15}$ may require rotation periods of $\lesssim$5 ms (Spruit 2002) or $\lesssim$25 ms (Fuller, Piro & Jermyn 2019), which make it a viable amplification mechanism for the Crab in the latter case.

4.2 Evolution of the supernova remnant

The low inferred explosion energies imply that the initial velocity of the ejecta was only a few hundred km s^{-1}, and that a majority of the kinetic energy of the current Crab ejecta is due to the acceleration of the ejecta by the pulsar wind nebula. In supernovae where the pulsar can deposit energy in excess of the initial supernova energy into the ejecta, the ram pressure of the ejecta cannot confine the pulsar bubble, leading the pulsar bubble to break out through the shell (Blondin & Chevalier 2017; Suzuki & Maeda 2017). This is the case over most of the posterior (see Fig. 3), but considering that some of the PWN escapes the system without interacting with the ejecta, the PWN energy that couples to the ejecta may be more comparable to the explosion energy.

The injected pulsar energy will cause the ejecta shell to become Rayleigh–Taylor unstable, leading to the formation of a filamentary structure similar to what is observed (Jun 1998; Bucciantini et al. 2004; Porth, Komissarov & Keppens 2014). The Rayleigh–Taylor instabilities create pressure waves that can deform, but not disrupt, the termination shock front (Camus et al. 2009; Porth et al. 2014); this may cause asymmetry in the photons emitted by the pulsar wind nebula but will not affect the large-scale structure of the remnant (Blondin & Chevalier 2017).

Simulations from Blondin & Chevalier (2017) show that once the pulsar wind nebula forward shock moves from the inner ejecta, with a flat density profile, to the outer ejecta, with a steep density profile ($\rho \overset{\propto}{\sim} r^{-9}$), the shock is strongly accelerated compared to the ejecta (see their fig. 5), leaving the most massive filaments behind. Given that the observed shock velocity is about a factor $\sim$2 greater than the velocity of the innermost filaments (Clark et al. 1983), fig. 5 from Blondin & Chevalier (2017) implies that the time when blowout started to occur must have been around 50–200 yr post-explosion. However, they use a constant spin-down luminosity instead of one that decreases with time, so this is only an upper limit.

For a constant pulsar spin-down, with $E_{\rm inj} = L_0 t$, we can put an independent, although speculative, constraint on the initial spin period of the pulsar. Using equation (6) from Blondin & Chevalier (2017) for the blowout time $t_{\rm tr}$, we find that $E_{\rm inj}/E_{\rm SN} = 1.5t/t_{\rm tr}$. Since $t/t_{\rm tr} \sim 10$ gives the value of the shock velocity consistent with the Crab, this implies that $E_{\rm inj}/E_{\rm SN} \sim 15$. If we assume that this is true regardless of the time dependence of the pulsar luminosity, that most of the rotational energy has already been emitted, and that the explosion energy is 10^{49-50} erg, then the initial rotational energy of the pulsar should be $\sim 1.5 \times 10^{50-51}$ erg. This is consistent with our Figs 2 and 3, but does exclude many of the slower rotating pulsars and a few of the fastest. The spin periods for these pulsars would be 4–13 ms.

This scenario also implies that the freely expanding ejecta outside the filaments cannot carry a significant amount of kinetic energy, and must therefore have a density profile that falls off more rapidly than r^{-4} (Sollerman et al. 2000). Further observations of the inner region of the Crab Nebula with sensitive, high-resolution instruments such as the JWST may help elucidate the low-velocity filament structure and the status of blowout within the nebula, placing further constraints on the energy injection of the Crab pulsar over the first few centuries of its lifetime.

The Crab is expanding within a low density void in the H I distribution (Romani et al. 1990; Wallace, Landecker & Taylor 1994; Wallace et al. 1999). The low ISM density means that the supernova forward and reverse shocks should be faint, which is consistent with their current non-detections (Mauche & Gorenstein 1989; Frail et al. 1995; Predehl & Schmitt 1995; Seward et al. 2006). Due to the low inferred explosion energy, the supernova forward and reverse shocks should have velocities not significantly higher than the 2500 km s^{-1} inferred from Sollerman et al. (2000).

4.3 Light echoes

The light associated with the luminous peak of the supernova can scatter off of dust clouds around the remnant, which can be detected after a time delay. These light echoes have been detected for several historical supernovae (Crotts, Kunkel & McCarthy 1989; Rest et al. 2005, 2008; Sugerman et al. 2006), and both Tycho's SN (Rest et al. 2008; Krause et al. 2008b) and Cas A (Rest et al. 2008, 2011a, b; Krause et al. 2008a) were able to be classified as a Type Ia and Type IIb SN, respectively, because of light echo spectroscopy. Despite its old age and low-density environment, it may be possible to detect light echoes from SN 1054 as well.

Detection of light echoes from SN 1054 could provide a direct test of the power source of the supernova. The brightness evolution of the light echo would provide a better sampled light curve than the historical observations. The presence or absence of a plateau would provide a diagnostic of whether the supernova was a Type II-P/IIn-P (Smith 2013) or something else, and better time resolution around the supernova peak would provide stronger constraints on the initial pulsar properties.

The spectrum in the early phase would also show slightly broader lines than the currently inferred filament and shock velocity due to the photosphere receding from the expanding envelope. These lines would likely have velocities around 2500 km s^{-1}, similar to that inferred by C IV absorption (Sollerman et al. 2000). Due to the slow, high-opacity ejecta, the transition to the nebular phase would likely take several years, so the narrowing of the lines as the photosphere recedes would likely not be detectable. The early spectrum would likely resemble an SLSN-II without narrow features (Kangas et al. 2022), showing broad Balmer emission lines, sometimes with a P Cygni profile, as well as absorption lines from Na I, He I, Fe II, Sc II and emission from Mg I] and Ca II. The spectrum may also develop H α and H β emission lines a few weeks after maximum light. The supernova would not be expected to show narrow hydrogen lines in this scenario, in contrast to a Type IIn or IIn-P.

4.4 Comparison with previous works

Several works have suggested that the Crab pulsar could have contributed to the luminosity of SN 1054 (Schramm 1977; Chevalier & Fransson 1992; Sollerman et al. 2001), but note that the pulsar wind

nebula would not be a significant source of supernova luminosity unless the nebula luminosity was orders of magnitude higher than it currently is. This would happen if either the pulsar was rapidly rotating (Atoyan 1999) or the magnetic field was much higher than it currently is, as we find.

SN 1054 was previously fit with a pulsar-driven model by Li et al. (2015), although their results and methodology are significantly different than ours. The most obvious difference is that they do not use a Bayesian inference code to do their fit, and thus cannot show parameter posteriors or show the uncertainty or correlation on their inferred values. They also used fixed values for several parameters, including gamma-ray opacity, ejecta mass, explosion energy, and distance, instead of marginalizing over them. They assume an electron scattering opacity of $\kappa = 0.2$ cm^2 g^{-1} instead of $\kappa = 0.34$ cm^2 g^{-1}, which is the standard value for hydrogen-rich supernovae. They also fix a temperature at peak and assume a bolometric correction for both epochs instead of self-consistently calculating what the observed emission would be in the human visual band.

The resulting spin periods measured by Li et al. (2015) are smaller than what we infer, although the spin-down time-scales are similar, implying a smaller magnetic field. The rotational energies inferred by their fits are $5 - 20\times 10^{50}$ erg, which are higher than our median value. Our inferred initial pulsar luminosity range is an order of magnitude lower, and their highest pulsar luminosity is similar to that inferred for an FBOT or BL-Ic SN (Omand & Sarin 2024). This extra energy causes their ejecta to expand much more rapidly than inferred either by our models or by observations.

An alternate scenario for explaining the properties of the Crab supernova and remnant is interaction with dense CSM ejected prior to the supernova, as detailed in Smith (2013). While an analysis of the pulsar + CSM scenario is beyond the scope of this work, and would likely not be useful due to a lack of observational constraints, it is worth noting how interaction would affect our inferred supernova and pulsar parameters. Since CSM interaction converts kinetic energy into radiated energy, the parameters would be consistent with a less luminous supernova with faster ejecta. There are two ways to achieve this, with vastly different implications implications on the evolution of the pulsar. One is that the magnetic field can increase even further, decreasing the spin-down time and supernova luminosity while increasing the ejecta velocity (Omand & Sarin 2024). The second is that the rotational energy can decrease, decreasing the supernova luminosity and ejecta velocity, with a corresponding increase to the supernova explosion energy to maintain or increase the velocity.

4.5 Comparison to other objects

The broad inferred spin period and magnetic field distributions and lack of many observational constraint make it difficult to determine what exactly the modern analogue of SN 1054 is. In particular, not having a strong constraint on the peak luminosity allows for possible analogues to range from normal Type II SNe, to luminous SNe (LSNe), to SLSNe, although we note that the boundaries between these classes are not well defined and there may simply be one continuous luminosity distribution.

SLSNe can show peak absolute magnitudes as faint as around -20 (Kangas et al. 2022; Chen et al. 2023a; Gomez et al. 2024), which is consistent with the most luminous light curves from the SN 1054 posterior sample. Sample studies of SLSNe-I tend to show spin periods $\lesssim$8 ms and dipole magnetic fields of $\sim$ 1–5 $\times$ 10^{14} G for spin periods $\gtrsim$4 ms, and $\sim$0.1–5 $\times$ 10^{14} G for spin periods $\lesssim$4 ms (Nicholl et al. 2017; Chen et al. 2023b). A sample study of SLSNe-II found similar parameters with spin periods $\lesssim$5 ms and dipole magnetic fields of $\sim$0.5–10 $\times$ 10^{14} G (Kangas et al. 2022). The majority of ejecta masses for both types of SLSNe are inferred to be between 3 and 10 $M_\odot$, similar to the possible range for SN 1054. These parameters are consistent with part of the distribution for SN 1054, although not with the mean inferred value, which has a similar magnetic field but slower spin period.

LSNe show peak absolute magnitudes between ~ -18 and -20 (Gomez et al. 2022; Pessi et al. 2023), which is more consistent with the majority of the SN 1054 posterior than SLSNe. The small sample of LSNe-II has no estimated pulsar parameters, and Pessi et al. (2023) prefer a CSM power source because of various other observational constraints. Gomez et al. (2022) present a sample of LSNe-I, and find the majority of them to have a significant contribution from a magnetar engine. The spin period and magnetic field distribution they find is broad, but does have several SNe with high magnetic field and slow spin period, similar to the inferred median initial values of the Crab pulsar. Rodríguez, Nakar & Maoz (2024) also claim that most stripped-envelope supernovae show signs of central engine activity at late times.

The progenitors of LSNe-I and SLSNe-I can vary greatly in mass due to the differing amount of material that can be stripped from the star before the explosion (Blanchard et al. 2020; Gomez et al. 2022). These SNe tend to be found is low-mass, star-forming galaxies (Lunnan et al. 2014; Leloudas et al. 2015; Angus et al. 2016; Schulze et al. 2018; Ørum et al. 2020), and are typically thought to come from progenitors with zero-age main-sequence (ZAMS) masses $\gtrsim$ 18 $M_\odot$ (Chen et al. 2023b), much larger than expected for SN 1054. For LSNe-II and SLSNe-II, the progenitors are expected to be less massive red supergiant (RSG) or yellow supergiant (YSG) stars (Kangas et al. 2022; Pessi et al. 2023), which is more consistent with the mass and composition expected for the progenitor of SN 1054.

5 SUMMARY

We use a model for a pulsar-driven supernova (Omand & Sarin 2024) to compare with historical and contemporary observations and constraints on the Crab supernova. We perform the fit using the Bayesian open-source software REDBACK (Sarin et al. 2024) and find that the most likely value for the initial spin-down luminosity is $\sim 10^{43-45.5}$ erg s^{-1} and for the initial pulsar spin-down time-scale is around 1–100 d. These imply an initial rotational energy of $\sim 10^{50}$ erg and an initial spin period of $\sim$14 ms. These also imply an initial magnetic field of $\sim 10^{14-15}$ G, which is orders of magnitude higher than the current characteristic magnetic field. The inferred bulk ejecta velocities are around 2000 km s^{-1}, which is similar to the current observed velocities of the PWN forward shock and filaments.

The large initial field implies that the magnetic field must have decayed over the lifetime of the pulsar. Ohmic dissipation along with vacuum dipole spin-down may be able to reproduce the inferred evolution, but may also require other spin-down and field dissipation mechanisms. The high initial rotational energy compared to the explosion energy means that the supernova probably underwent pulsar bubble blowout, which causes the PWN forward shock to accelerate and leave behind the material in the filaments. The slow PWN shock velocity gives an independent, although speculative, spin period constraint of 4–13 ms. The pulsar-driven scenario could be tested and constrained with light echo photometry and spectroscopy, particularly around the supernova peak. SN 1054 shares similarities with both hydrogen-rich and hydrogen-poor LSNe and SLSNe, giving it a wide range of possible modern analogues.

ACKNOWLEDGEMENTS

The authors thank the anonymous referee for their helpful comments. The authors also thank Jesper Sollerman for his helpful discussions. CMBO acknowledges support from the Royal Society (grant nos. DHF-R1-221175 and DHF-ERE-221005). NS acknowledges support from the Knut and Alice Wallenberg Foundation through the 'Gravity Meets Light' project. TT acknowledges support from the NSF grant AST-2205314 and the NASA ADAP award 80NSSC23K1130.

DATA AVAILABILITY

The model is available for public use within REDBACK (Sarin et al. 2024).

REFERENCES

Angus C. R., Levan A. J., Perley D. A., Tanvir N. R., Lyman J. D., Stanway E. R., Fruchter A. S., 2016, MNRAS, 458, 84
Ashton G. et al., 2019, ApJS, 241, 27
Atoyan A. M., 1999, A&A, 346, L49
Barrère P., Guilet J., Reboul-Salze A., Raynaud R., Janka J.-H., 2022, A&A, 668, A79
Barrère P., Guilet J., Raynaud R., Reboul-Salze A., 2023, MNRAS, 526, L88
Bietenholz M. F., Kronberg P. P., Hogg D. E., Reboul-Salze A., 1991, ApJ, 373, L59
Blanchard P. K., Berger E., Nicholl M., Ashley V. A., 2020, ApJ, 897, 114
Blondin J. M., Chevalier R. A., 2017, ApJ, 845, 139
Borghese A., 2023, Proc. IAU Symp. 363, Neutron Star Astrophysics at the Crossroads: Magnetars and the Multimessenger Revolution. Kluwer, Dordrecht, p. 51
Bucciantini N., Amato E., Bandiera R. et al., 2004, A&A, 423, 253
Buchner J. et al., 2014, A&A, 564, A125
Bühler R., Blandford R., 2014, Rep. Prog. Phys., 77, 066901
Callis E. et al., 2021, preprint (arXiv:2109.12943)
Camus N. F., Komissarov S. S., Bucciantini N., Hughes P. A., 2009, MNRAS, 400, 1241
Chen T. W. et al., 2021, preprint (arXiv:2109.07942)
Chen Z. H. et al., 2023a, ApJ, 943, 41
Chen Z. H. et al., 2023b, ApJ, 943, 42
Chevalier R. A., Fransson C., 1992, ApJ, 395, 540
Clark D. H., Stephenson F. R., 1977. The Historical Supernovae, Pergamon Press, New York, U.S.A
Clark D. H., Murdin P., Wood R., Gilmozzi R., Danziger J., Furr A. W., 1983, MNRAS, 204, 415
Collins G. W. II, Claspy W. P., Martin J. C., 1999, PASP, 111, 871
Crotts A. P. S., Kunkel W. E., McCarthy P. J., 1989, ApJ, 347, L61
Davidson K., Fesen R. A., 1985, ARA&A, 23, 119
Dessart L., 2019, A&A, 621, A141
Dessart L., Hillier D. J., Li C., Woosley S., 2012, MNRAS, 424, 2139
Dexter J., Kasen D., 2013, ApJ, 772, 30
Eftekhari T. et al., 2019, ApJ, 876, L10
Eftekhari T. et al., 2021, ApJ, 912, 21
Fesen R. A., Shull J. M., Hurford A. P., 1997, AJ, 113, 354
Frail D. A., Kassim N. E., Cornwell T. J., Goss T. M., 1995, ApJ, 454, L129
Fuller J., Piro A. L., Jermyn A. S., 2019, MNRAS, 485, 3661
Gomez S., Berger E., Nicholl M., Blanchard P. K., Hosseinzadeh G., 2022, ApJ, 941, 107
Gomez S. et al., 2024, MNRAS, 535, 471
Guilet J., Reboul-Salze A., Raynaud R., Bugli M., Gallet B., 2022, MNRAS, 516, 4346
Hachinger S., Mazzali P. A., Taubenberger S., Hillebrandt W., Nomoto K., Sauer D. N., 2012, MNRAS, 422, 70
Hester J. J., 2008, ARA&A, 46, 127
Hiramatsu D. et al., 2021, Nat. Astron., 5, 903
Igoshev A. P., Popov S. B., Hollerbach R., 2021, Universe, 7, 351
Inserra C., Bulla M., Sim S. A., Smartt S., 2016, ApJ, 831, 79
Inserra C. et al., 2018, MNRAS, 475, 1046
Jerkstrand A. et al., 2017, ApJ, 835, 13
Jun B.-I., 1998, ApJ, 499, 282
Kangas T. et al., 2022, MNRAS, 516, 1193
Kitaura F. S., Janka H. T., Hillebrandt W., 2006, A&A, 450, 345
Kou F. F., Tong H., 2015, MNRAS, 450, 1990
Krause O., Birkmann S. M., Usuda T., Hattori T., Goto M., Rieke G. H., Misselt K., 2008a, Science, 320, 1195
Krause O., Tanaka M., Usuda T., Hattori T., Goto M., Birkmann S., Nomoto K., 2008b, Nature, 456, 617
Lasky P. D., Leris C., Rowlinson A., Glampedakis K., 2017, ApJ, 843, L1
Law C. J. et al., 2019, ApJ, 886, 24
Leloudas G. et al., 2015, MNRAS, 449, 917
Li S.-Z., Yu Y.-W., Huang Y., 2015, Res. Astron. Astrophys., 15, 1823
Lin R., van Kerkwijk M. H., Kirsten F., Pen U.-L., Deller D. T., 2023, ApJ, 952, 161
Lunnan R. et al., 2014, ApJ, 787, 138
Lyne A. G., Pritchard R. S., Graham Smith F., 1993, MNRAS, 265, 1003
Lyne A. G., Jordan C. A., Graham-Smith F., Espinoza M. C., Stappers B. W., Weltevrede P., 2015, MNRAS, 446, 857
MacAlpine G. M., McGaugh S. S., Mazzarella J. M., Uomoto A., 1989, ApJ, 342, 364
Manchester R. N., Hobbs G. B., Teoh A., Hobbs M., 2005, AJ, 129, 1993
Margutti R. et al., 2023, ApJ, 954, L45
Mauche C. W., Gorenstein P., 1989, ApJ, 336, 843
Melatos A., 1999, ApJ, 519, L77
Metzger B. D., 2019, Living Rev. Relat., 23, 1
Miller J. S., 1973, ApJ, 180, L83
Miyaji S., Nomoto K., Yokoi K., Sugimoto D., 1980, PASJ, 32, 303
Mondal S., Bera A., Chandra P., Bartos I., 2020, MNRAS, 498, 3863
Murase K., Kashiyama K., Kiuchi K., Bartos I., 2015, ApJ, 805, 82
Nicholl M., Guillochon J., Berger E., 2017, ApJ, 850, 55
Nomoto K., 1987, ApJ, 322, 206
Nomoto K., Sparks W. M., Fesen R. A., Gull T. R., Miyaji S., 1982, Nature, 299, 803
Omand C. M. B., Jerkstrand A., 2023, A&A, 673, A107
Omand C. M. B., Sarin N., 2024, MNRAS, 527, 6455
Omand C. M. B., Kashiyama K., Murase K., 2018, MNRAS, 474, 573
Omand C. M. B., Kashiyama K., Murase K., 2019, MNRAS, 484, 5468
Ørum S. V., Ivens D. L., Strandberg P., Leloudas G., Man A. W. S., Schulze S., 2020, A&A, 643, A47
Owen P. J., Barlow M. J., 2015, ApJ, 801, 141
Pacini F., 1967, Nature, 216, 567
Pessi P. J. et al., 2023, MNRAS, 523, 5315
Pitkin M., 2018, J.Source Softw., 3, 538
Poidevin F., Omand C. M. B., Pérez-Fournon I., Clavero R., Shirley R., Marques-Chaves R., Angel Jimenez C., Geier S., 2022, MNRAS, 511, 5948
Poidevin F. et al., 2023, MNRAS, 521, 5418
Pons J. A., Geppert U., 2007, A&A, 470, 303
Popov D. V., 1993, ApJ, 414, 712
Porth O., Komissarov S. S., Keppens R., 2014, MNRAS, 443, 547
Predehl P., Schmitt J. H. M. M., 1995, A&A, 293, 889
Pursiainen M. et al., 2022, A&A, 666, A30
Pursiainen M. et al., 2023, A&A, 674, A81
Raynaud R. et al., 2020, Sci. Adv., 6, eaay2732
Reboul-Salze A., Guilet J., Raynaud R., Bugli M., 2021, A&A, 645, A109
Reboul-Salze A., Guilet J., Raynaud R., Bugli M., 2022, A&A, 667, A94
Rest A. et al. 2005, Nature, 438, 1132
Rest A. et al., 2008, ApJ, 681, L81
Rest A., Sinnott B., Welch D. L., Foley R. J., Narayan G., Mandel K., Huber M. E., Blondin S., 2011a, ApJ, 732, 2
Rest A. et al., 2011b, ApJ, 732, 3
Rodríguez Ó., Nakar E., Maoz D., 2024, Nature, 628, 733
Romani R. W., Reach W. T., Koo B. C., Heiles C., 1990, ApJ, 349, L51
Saito S. et al., 2020, ApJ, 894, 154
Sarin N., Lasky P. D., Sammut L., Greg A., 2018, Phys. Rev. D, 98, 043011

Sarin N., Lasky P. D., Ashton G., 2020, Phys. Rev. D, 101, 063021
Sarin N., Omand C. M. B., Margalit B., Jones D. I., 2022, MNRAS, 516, 4949
Sarin N., Brandenburg A., Haskell B., 2023, ApJ, 952, L21
Sarin N. et al., 2024, MNRAS, 531, 1203
Schramm D., 1977, Supernovae. D. Reidel Publishing Company, Dordrecht, Holland
Schulze S. et al., 2018, MNRAS, 473, 1258
Seward F. D., Gorenstein P., Smith R. K., 2006, ApJ, 636, 873
Smith N., 2003, MNRAS, 346, 885
Smith N., 2013, MNRAS, 434, 102
Sollerman J. et al., 2000, ApJ, 537, 861
Sollerman J., Kozma C., Lundqvist P., 2001, A&A, 366, 197
Spruit H. C., 2002, A&A, 381, 923
Staelin D. H., Reifenstein E. C. III, 1968, Science, 162, 1481
Sugerman B. E. K. et al., 2006, Science, 313, 196
Sun L., Xiao L., Li G., 2022, MNRAS, 513, 4057
Suzuki A., Maeda K., 2017, MNRAS, 466, 2633
Temim T. et al., 2006, AJ, 132, 1610
Temim T. et al., 2024, ApJ, 968, L18
Tsuna D., Matsumoto T., Wu S. C., Fuller J.,2024, ApJ, 966, 30
Vurm I., Metzger B. D., 2021, ApJ, 917, 77
Wallace B. J., Landecker T. L., Taylor A. R., 1994, A&A, 286, 565
Wallace B. J., Landecker T. L., Kalberla P. M. W., Taylor A. R., 1999, ApJS, 124, 181
Wang S. Q. et al., 2015, ApJ, 799, 107
Yang H., Chevalier R. A., 2015, ApJ, 806, 153
Yu Y.-W., Zhang B., Gao H., 2013, ApJ, 776, L40
Zhang J. et al., 2020, MNRAS, 498, 84

APPENDIX A: PARAMETER POSTERIORS FOR SN 1054

The full posterior for all inferred parameters when assuming $n = 3$ is shown in Fig. A1, the posterior when assuming the current Crab value of $n = 2.51$ is shown in A2, and the posterior when assuming $n = 3$ and $T_{\rm min} = 6000$ K (around the recombination temperature for hydrogen) is shown in Fig. A3. The three posteriors show extremely similar behaviour, verifying that our results are not strongly affected by these assumptions.. The posteriors for ejecta mass, explosion energy, and distance are almost flat, meaning that little information about these properties can be derived from the light curve. The posteriors for explosion time and gamma-ray opacity all tend towards lower values, but are still broad enough that the value we infer is not well constrained. The temperature when the photosphere recedes is well constrained to around $\sim$ 3000–4000 K.

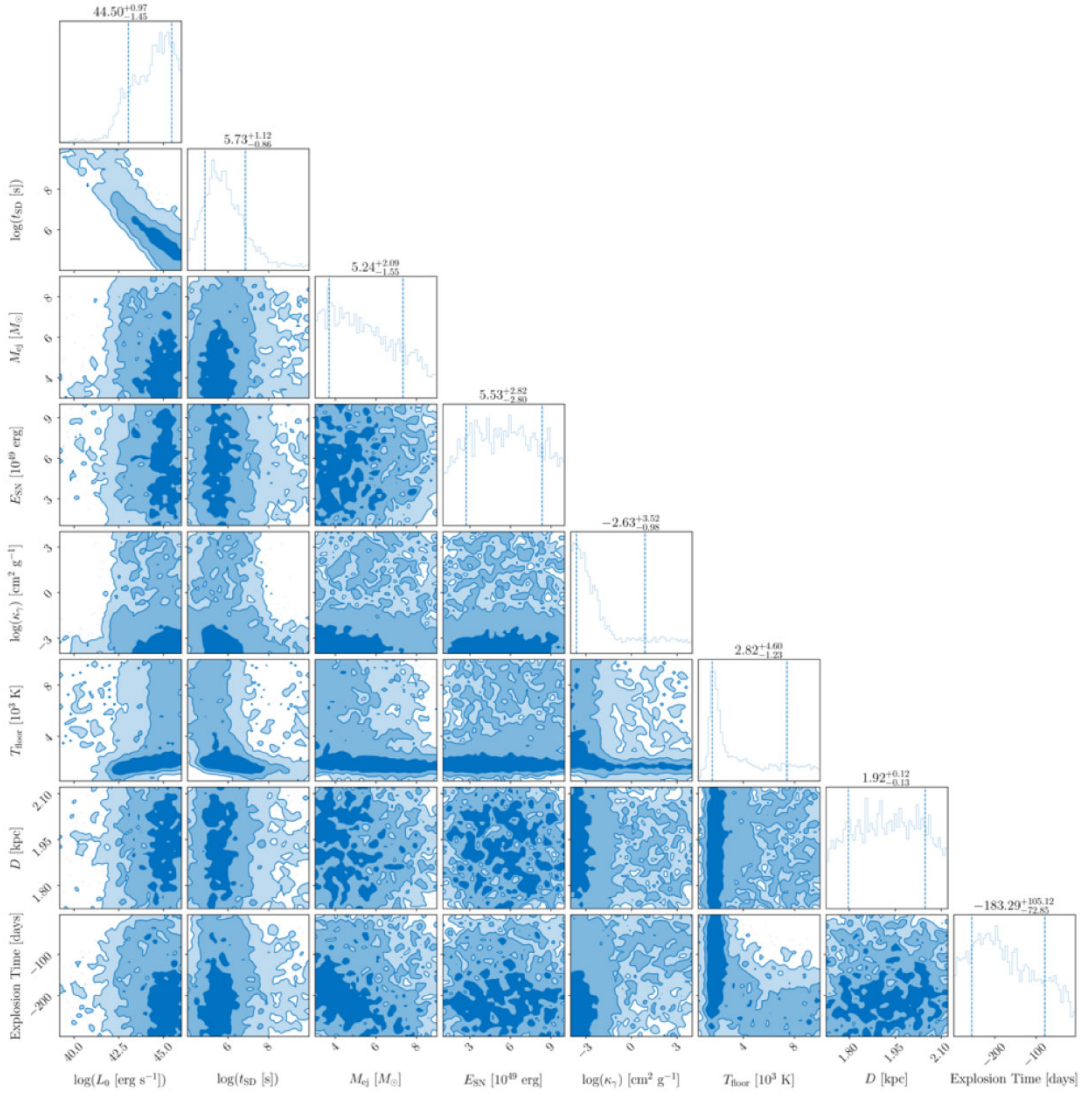

Figure A1. Posterior distribution of parameters inferred for SN 1054 for $n = 3$. The explosion time is from when the supernova fades from the daytime sky.

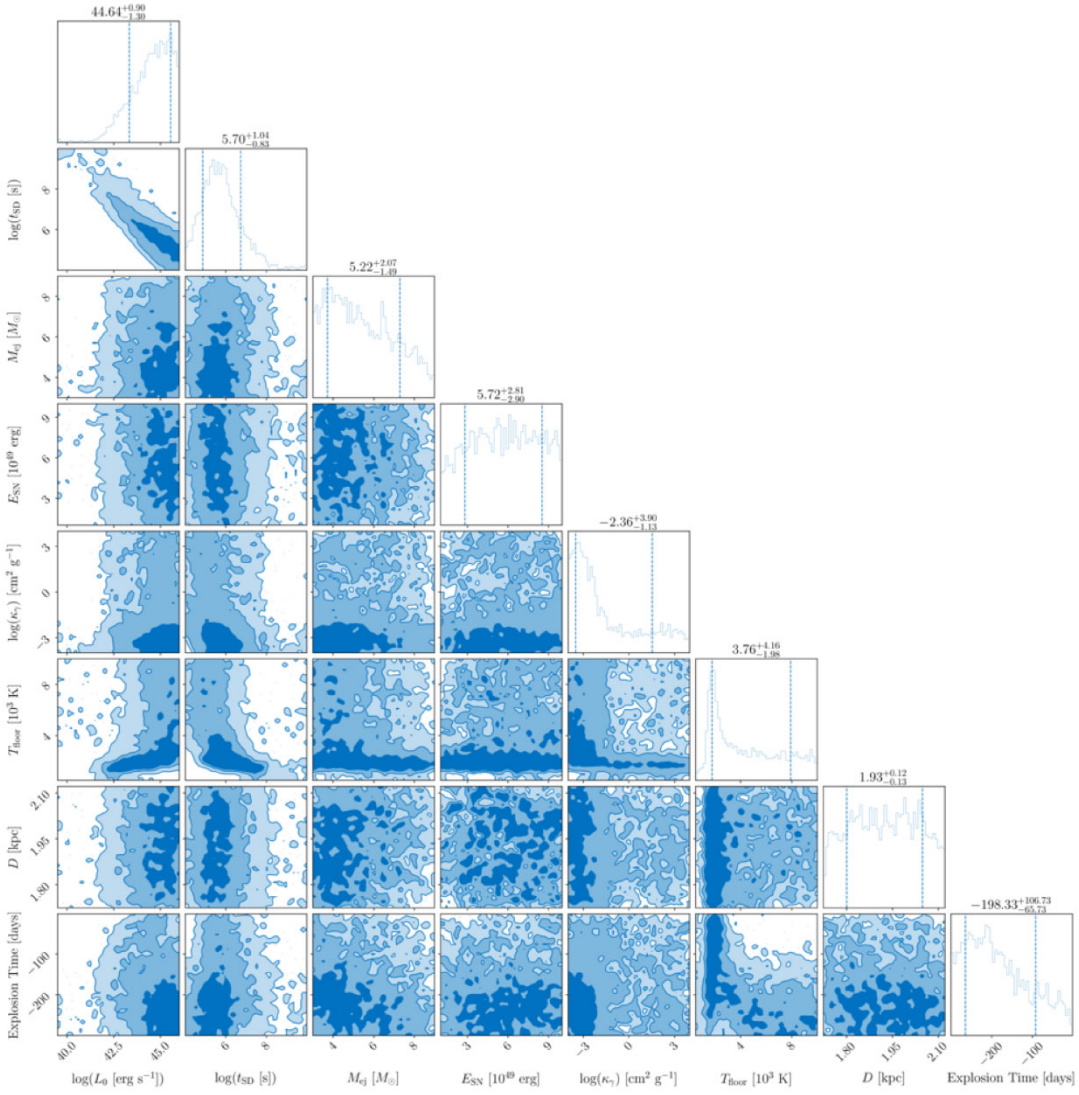

Figure A2. Posterior distribution of parameters inferred for SN 1054 for $n = 2.51$. The explosion time is from when the supernova fades from the daytime sky.

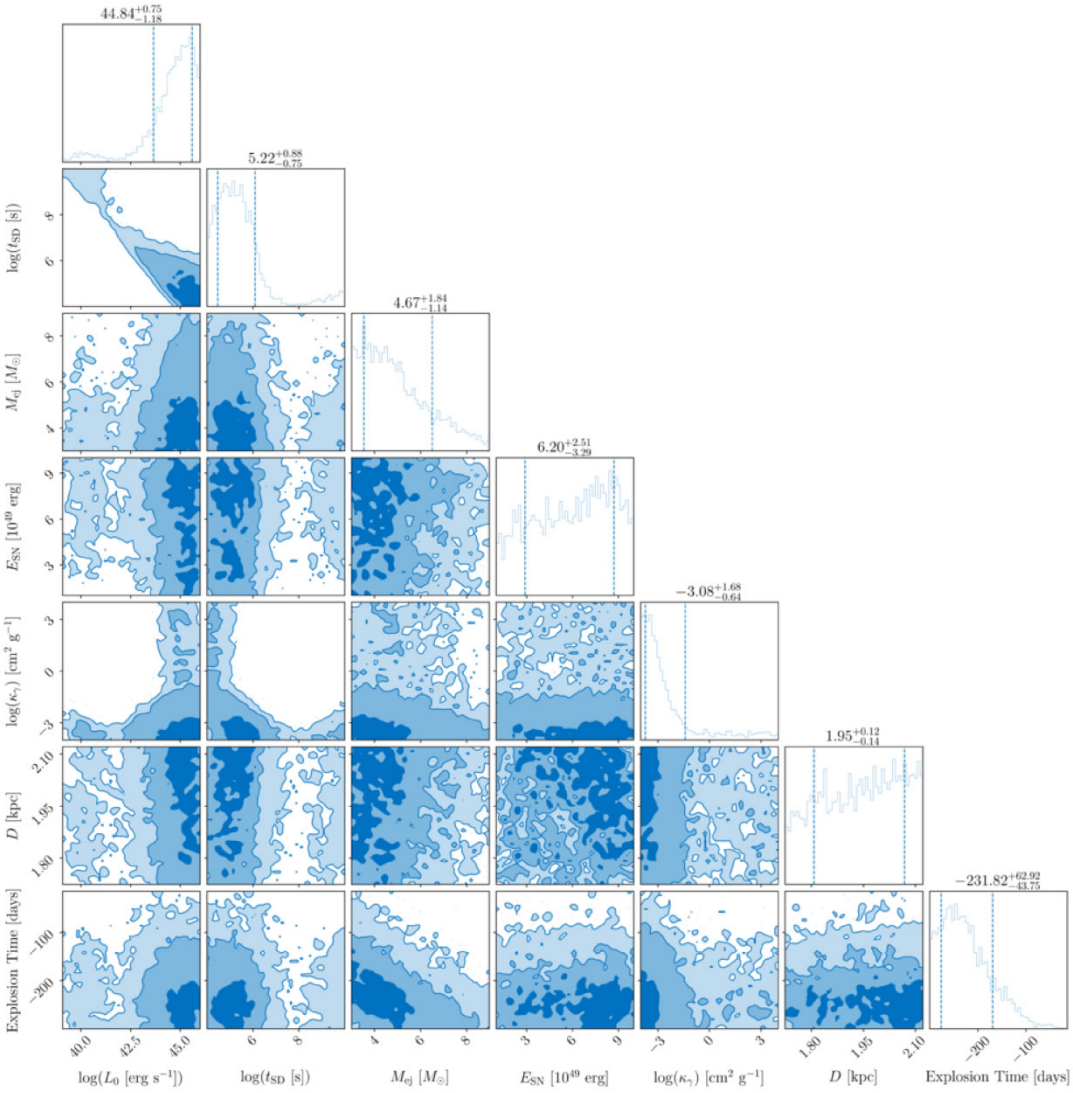

Figure A3. Posterior distribution of parameters inferred for SN 1054 for $n = 3$ and $T_{\rm min}$ fixed to 6000 K. The explosion time is from when the supernova fades from the daytime sky.

APPENDIX B: ANALYTICAL ESTIMATION OF INITIAL SPIN FREQUENCY

We can take a simple extrapolation from only currently observed values to derive an estimate of the initial spin period. By taking the equation for spin down

$$\dot{\nu} = -k\nu^n, \tag{B1}$$

and assuming constant k and braking index n, we can get an estimate of the initial spin period of the pulsar. Solving for ν and $\dot{\nu}$ gives

$$\nu = \left[(n-1)(C_1 + kt)\right]^{\frac{1}{1-n}}, \tag{B2}$$

$$\dot{\nu} = -k\left[(n-1)(C_1 + kt)\right]^{\frac{n}{1-n}}, \tag{B3}$$

where C_1 is an integration constant. Taking the ratio $\nu/\dot{\nu}$ gives

$$\nu/\dot{\nu} = -\frac{n-1}{k}(C_1 + kt), \tag{B4}$$

$$\frac{C_1}{k} = -\left(\frac{\nu}{\dot{\nu}(n-1)} + t\right). \tag{B5}$$

Solving equation (B5) at $t = 939$ yr with the Crab spin frequency $\nu = 30.2$ Hz and spin frequency derivative $\dot{\nu} = -3.86 \times 10^{-10}$ Hz s^{-1} (Lyne et al. 1993) gives $C_1/k = 2.25 \times 10^{10}$ s. Substituting this for into equation (B2) at $t = 939$ yr allows us to solve for C_1,

$$C_1 = \frac{\nu^{1-n}}{n-1}\left(1 + \frac{t}{C_1/k}\right)^{-1} = 1.7 \times 10^{-3}, \tag{B6}$$

for $n = 2.5$. Then, solving for ν at $t = 0$ gives the initial spin frequency

$$\nu_0 = ((n-1)C_1)^{\frac{1}{1-n}} = 53 \text{ Hz}, \tag{B7}$$

corresponding to an initial spin period of 19 ms. Repeating the above calculation with $n = 3$ gives a spin frequency of 61 Hz, or spin period of 16 ms.

The initial pulsar conditions derived here would have a luminosity too low to power the observed supernova light curve, implying that the assumption of constant k and n is incorrect if the pulsar-driven scenario is correct. This shows the importance of accounting for the historical supernova data when estimating the initial conditions of the Crab pulsar.

This paper has been typeset from a TEX/LATEX file prepared by the author.